Biochimica et Biophysica Acta 1837 (2014) 396–405

Contents lists available at ScienceDirect

Biochimica et Biophysica Acta

journal homepage: www.elsevier.com/locate/bbabio

Structural and functional characterization of the *Geobacillus* copper nitrite reductase: Involvement of the unique N-terminal region in the interprotein electron transfer with its redox partner ☆

Yohta Fukuda [a,b,c,1], Hiroyasu Koteishi [a,1,2], Ryohei Yoneda [a], Taro Tamada [c], Hideto Takami [d], Tsuyoshi Inoue [b], Masaki Nojiri [a,e,*]

[a] Department of Chemistry, Graduate School of Science, Osaka University, 1-1 Machikaneyama, Toyonaka, Osaka 560-0043, Japan
[b] Department of Materials Chemistry, Graduate School of Engineering, Osaka University, Suita, Osaka 565-0871, Japan
[c] Molecular Biology Research Center, Quantum Beam Science Directorate, Japan Atomic Energy Agency, Tokai, Ibaraki 319-1195, Japan
[d] Microbial Genome Research Group, Japan Agency of Marine-Earth Science and Technology, Yokosuka, Kanagawa 237-0061, Japan
[e] RIKEN SPring-8 Center, 1-1-1 Kouto, Sayo, Hyogo 679-5148, Japan

ARTICLE INFO

Article history:
Received 17 September 2013
Received in revised form 19 December 2013
Accepted 7 January 2014
Available online 14 January 2014

Keywords:
Denitrification
Electron transfer
Copper nitrite reductase
Cytochrome *c*
X-ray crystallography

ABSTRACT

The crystal structures of copper-containing nitrite reductase (CuNiR) from the thermophilic Gram-positive bacterium *Geobacillus kaustophilus* HTA426 and the amino (N)-terminal 68 residue-deleted mutant were determined at resolutions of 1.3 Å and 1.8 Å, respectively. Both structures show a striking resemblance with the overall structure of the well-known CuNiRs composed of two Greek key β-barrel domains; however, a remarkable structural difference was found in the N-terminal region. The unique region has one β-strand and one α-helix extended to the northern surface of the type-1 copper site. The superposition of the *Geobacillus* CuNiR model on the electron-transfer complex structure of CuNiR with the redox partner cytochrome c_{551} in other denitrifier system led us to infer that this region contributes to the transient binding with the partner protein during the interprotein electron transfer reaction in the *Geobacillus* system. Furthermore, electron-transfer kinetics experiments using N-terminal residue-deleted mutant and the redox partner, *Geobacillus* cytochrome c_{551}, were carried out. These structural and kinetics studies demonstrate that the region is directly involved in the specific partner recognition.

1. Introduction

In the absence of oxygen, nitrate (NO_3^-) can be used by many microbes as an alternative respiratory electron acceptor. Nitrate reduction is coupled to the anaerobic oxidation of organic carbon, producing either NH_4^+ in a process known as dissimilatory nitrate reduction to ammonium (DNRA) or, more commonly, N_2 gas during denitrification [1]. Denitrifiers include representatives of more than 60 genera of bacteria and archaea, as well as some eukaryotes (e.g., fungi, protozoa, and benthic Foraminifera and Gromiida) [2,3]. Generally, the process involves four metalloenzymes: dissimilatory nitrate reductase, nitrite reductase, nitric oxide reductase, and nitrous oxide reductase [4]. It is the only process in which the major end product is removed from the internal biological nitrogen cycle, being the principal means of balancing the input flux from biological nitrogen fixation. It has been known that the rate-limiting step in denitrification is the nitrite reduction to nitric oxide, being a key step for effective process [4,5].

Copper-containing nitrite reductase (CuNiR) catalyzes the one-electron reduction of nitrite (NO_2^-) to nitric oxide (NO), which is the committing step in the denitrification process. Generally, this enzyme has a homotrimeric structure organized in three identical subunits composed of two Greek key β-barrel cupredoxin domains [6]. Six Cu atoms are located in the trimeric CuNiR molecule and could be classified into the following two Cu types. The type-1 copper site (T1Cu) is buried within the N-terminal cupredoxin domain in the monomeric subunit and is coordinated by four residues (i.e., two His, Cys, and Met) being responsible for the blue- or green-color of the CuNiR [7]. T1Cu plays a role in the electron delivery from the physiological redox-partner protein to the type-2 copper site (T2Cu) located at the interface between the

Abbreviations: CuNiR, copper-containing nitrite reductase; GkNiR, CuNiR from *Geobacillus kaustophilus*; AxNiR, CuNiR from *Achromobacter xylosoxidans*; Cyt c_{551}, cytochrome c_{551}; GkCyt c_{551}, Cyt c_{551} from *Geobacillus kaustophilus*; AxCyt c_{551}, Cyt c_{551} from *Achromobacter xylosoxidans*; T1Cu, type 1 copper site; T2Cu, type 2 copper site; wt, wild-type; ET, electron transfer; SDS-PAGE, sodium dodecyl sulfate-polyacrylamide gel electrophoresis; EDTA, ethylenediaminetetraacetic acid; Tris, tris (hydroxymethyl) aminomethane; RMS, root-mean-square

☆ Atomic coordinates for wt GkNiR and Δ1-68 mutant have been deposited in the Protein Data Bank with accession codes: 3WI9 (wt GkNiR) and 3WIA (Δ1-68 mutant).

* Corresponding author at: Department of Chemistry, Graduate School of Science, Osaka University, 1-1 Machikaneyama, Toyonaka, Osaka 560-0043, Japan. Tel.: +81 6 6850 5768; fax: +81 6 6850 5787.
E-mail address: nojiri@ch.wani.osaka-u.ac.jp (M. Nojiri).
[1] These authors contributed equally to this work.
[2] Present address: Laboratory for Cell Signaling Dynamics, RIKEN Quantitative Biology Center, Suita, Japan.

0005-2728/$ – see front matter © 2014 Elsevier B.V. All rights reserved.
http://dx.doi.org/10.1016/j.bbabio.2014.01.004

adjacent subunits in the trimer. T2Cu is coordinated by three His residues and serves as the site for nitrite binding and reduction. The two Cu sites are about 12.5 Å apart but are connected via the His-Cys sequence segment composed of the Cys residue of T1Cu and His residue of T2Cu [6].

CuNiR is further classified into two groups, Class-I and II, on the basis of the length of the two surface loops, which are the "Linker" loop connecting two cupredoxin domains in the monomeric subunit and the "Tower" loop positioned near the T1Cu [8]. The CuNiR from *Neisseria gonorrhoeae* (NgNiR), the first Class-II CuNiR investigated in detail using X-ray crystallography, has the shortest Linker and Tower loops among those found in CuNiRs. Paramagnetic nuclear magnetic resonance (NMR) spectroscopic and X-ray crystallographic studies for the transient electron transfer (ET) complex of CuNiR with its redox-partner protein have demonstrated that the redox-partner proteins interact with the hydrophobic patch on the T1Cu near the Tower loop region [9,10]. It has been suggested that the Tower loop region contributes greatly to the recognition for the partner proteins. Recently, the crystal structures of the natural fusion types of CuNiR tethering the redox-partner proteins have been also reported [11–13]. The structures also support the idea that structural features at the surface near T1Cu are important for transient interaction between the redox partners.

Recent genomic and bioinformatic studies have revealed the presence of the gene clusters associated with denitrification in the thermophilic Gram-positive *Geobacillus* species [14]. Although several Gram-positive denitrifiers have been characterized in the past, there is still uncertainty about the occurrence of the denitrification trait among these bacteria [15]. The amino acid sequence deduced from the *nirK* gene encoding for CuNiR (UniProt code: Q5L1X8) in *Geobacillus kaustophilus* HTA426 shows relatively low similarity (~30%) to the well-known Class-I and II CuNiRs, although the residues for the Cu-binding sites are well conserved. The *ClustalW*-alignment analysis reveals the presence of the three characteristic loop regions in the amino acid sequences of *Geobacillus* CuNiRs, which include not only the "Linker" and "Tower" loops but also the "Extra" loop [16]. This finding prompts the speculation that *Geobacillus* CuNiRs adapt commonly to the environmental stresses by some conformational changes mediated by amino acid replacement, deletion, and/or insertion. Moreover, for a deeper atomic-level understanding of the adaptive evolution of the CuNiR molecule, it is essential to determine and analyze the three-dimensional structure of *Geobacillus* CuNiR.

Herein we describe the high-resolution crystal structure of GkNiR and then focus the unique N-terminal structure coupled with some loop structures at near the T1Cu site. Using stopped-flow kinetics with the cognate cytochrome c_{551} (GkCyt c_{551}, UniProt code: Q5KV99) as a possible redox-partner for GkNiR, it has been demonstrated that the N-terminal region of GkNiR greatly contributes to the partner recognition during the interprotein ET reaction between GkNiR and GkCyt c_{551}. Based on these data, the possible adaptive evolutions of not only the thermophilic GkNiR molecule structure, but also the interprotein ET reaction with the redox-partner protein are discussed.

2. Materials and methods

2.1. Bacterial strains and plasmids

Escherichia coli strains DH5α (Invitrogen) and Rosetta-gami (DE3) (Merck) were used for cloning and expression, respectively. Cultures were grown in Luria–Bertani (LB) medium or on LB-agar plates. The growth media were supplemented with ampicillin (200 μg/mL) and, where appropriate, chloramphenicol (34 μg/mL). The plasmid pEC86, a derivative of pACYC184, containing the *ccm* gene cluster [17] was a kind gift from Dr. J.M. Stevens (University of Oxford, UK).

2.2. Cloning, expression, and purification of CuNiR and Cyt c_{551}

The *nirK* gene from *G. kaustophilus* HTA426 was previously cloned into the pET-20b (+) vector (Merck) between the *Nde*I and *Hin*dIII restriction sites [16]. Moreover, the *nirK* gene from *Achromobacter xylosoxidans* GIFU1051 was cloned into the pMal-c2x vector (New England Biolab) between the *Xmn*I and *Bam*HI restriction sites [18]. Their expression and purification protocols were the same to the procedures described previously [16,18].

The gene encoding the putative soluble region (between residues Ala26 and Lys111 of GK3102) annotated with the cytochrome c_{551} gene was amplified by PCR using the genomic DNA of *G. kaustophilus* HTA426 as the template. The N-terminal region from Met1 to Asn25 was predicted to act as a signal peptide for secretion by using the amino acid sequence-based predictor server SignalP4.1 (http://www.cbs.dtu.dk/services/SignalP/) [19]. Moreover, the lipo-box motif [20] for the lipid-modified cysteine site ($L^{16}AA\mathbf{C}^{19}$), functioning as an anchor into the cell membrane, was also found in this region. In this study the N-terminal region was replaced with the *pelB* leader peptide [21] from the pET-20b (+) vector by genetic engineering to achieve an efficient over-production in *E. coli*. The restriction enzymes sites for *Nco*I (CCATGG) and *Hind*III (AAGCTT) sites were incorporated into the sequences of the forward and reverse primers, 5′-TT**CCATGG**CCGGGGAGAAAAAC GACGCAGC-3′ and 5′-AT**AAGCTT**ATTTTTTCGCAGCCAGCCATTCCG-3′, respectively. The DNA product fragment was cloned into pET-20b (+) opened by digestion with *Nco*I and *Hind*III. The presence of the insert was confirmed by DNA-sequence analysis. The *pelB* leader peptide (Met1 to Met23) was added before the Ala26 residue of GkCyt c_{551}, and the peptide was digested before Met23 with an *E. coli* signal peptidase for secretion into the periplasm.

Furthermore, the gene encoding the region from Ala27 to Arg108 of NirM (AxCyt c_{551}) from *A. xylosoxidans* GIFU1051 [10] was also amplified by PCR using the cognate genomic DNA as the template. The N-terminal region (Met1 to Pro26) was replaced with the *pelB* leader peptide from the pET-20b (+) vector to achieve an efficient over-production in *E. coli*. The restriction enzymes *Nco*I (CCATGG) and *Hind*III (AAGCTT) sites were incorporated into the sequences of the forward and reverse primers, 5′-CC**CCATGG**CCCAGCTCGACCCGGCCGGTGAAAA-3′ and 5′-CC**AAGCTT**AGCGCGCGGCGTCCATCATGTAC-3′, respectively. The DNA product fragment was cloned into the pET-20b (+) opened by digestion with *Nco*I and *Hind*III. As a result, the *pelB* leader peptide from Met1 to Met23 was added before the Ala27 of AxCyt c_{551}.

For both Cyt c_{551} sequences, the expression strains were co-transformed with plasmid pEC86 [17]. The proteins were produced in *E. coli* strain Rosetta-gami (DE3). The expression protocols were the same in both cases, and 100 μM IPTG was used for induction. For the purification of GkCyt c_{551}, the harvested cells were resuspended in 40 mM Tris–HCl buffer (pH 8.0) containing 0.5 mM phenylmethanesulfonyl fluoride. The suspension was sonicated at 160 W for 30 min, and the debris was removed by centrifugation at 15,000 rpm for 1 h at 4 °C. Ammonium sulfate (AS) was added to 35%-saturated concentration to the supernatant, and the resulting precipitate was separated by centrifugation. The supernatant was loaded onto a Phenyl-Sepharose Fast Flow column (2.5 cm × 25 cm; GE Healthcare) pre-equilibrated with 40 mM Tris–HCl buffer (pH 8.0) containing a 35% saturated concentration of AS. After washing the column with 1 L of the same buffer, the red-colored cytochromes were eluted with a linear gradient from 35% to 0% saturated AS in the same buffer. The cytochrome-containing fractions were collected and dialyzed against 40 mM Tris–HCl buffer (pH 8.0) containing 20% AS. After removing the precipitate by centrifugation, the supernatant was loaded onto an HPLC hydrophobic Phenyl-5PW column (0.9 × 5.0 cm; Tosoh) pre-equilibrated with 40 mM Tris–HCl buffer (pH 8.0) containing 20% AS. The single hemoprotein was then eluted with a linear gradient from 20% to 0% AS. The fractions were collected, concentrated, and desalted with a Centriprep-YM3 device (Millipore). The purity, estimated by SDS-PAGE and spectrophotometrically, was

observed to be >95%. In addition, AxCyt c_{551} was purified by cation exchange and hydrophobic column chromatography according to the procedures described previously [22].

2.3. Construction and preparation of the GkNiR Mutants

Two GkNiR mutants with a deletion of the N-terminal amino acid residues from 1 to 51 and 1 to 68, Δ1-51 and Δ1-68, were constructed. They were obtained by a PCR method using the following primers; 5′-TA**CATATG**CACAAAAGGGGTGAATCAAGCACCGG-3′ for Δ1-51 and 5′-TA**CATATG**CCTCATGATGTCCACATCGAAATGACA-3′, for Δ1-68. The reverse primers for the PCRs were the same as those used in a previous report detailing the construction of wt GkNiR [16]. The PCR products of two mutants were digested with *Nde*I and *Hin*dIII, and then cloned into the expression vector pET20-b (+) opened by digestion with the same restriction enzymes. The expression and purification protocols were the same for wt GkNiR [16].

2.4. X-ray crystallography

The initial model for wt GkNiR by molecular replacement using the NgNiR model (PDB ID: 1KBW) as a search model has been constructed previously [8,16]. At the second stage, a difference Fourier electron density map with sufficient quality was produced for building the omitted residues into the density maps using Coot [23]. At a later stage, Refmac5 was used for refinement, and the solvent molecules were gradually included in the model [24]. The model was then thoroughly examined for possible errors using both maps at contour levels of 1.5σ ($2F_O - F_C$) and $\pm 4.0\sigma$ ($F_O - F_C$). Only those solvent molecules with thermal parameters of <60 Å^2 and reasonable hydrogen-bonding properties were included in the model. The structure was refined to *R*-factor and *R*-free values of 0.18 and 0.19, respectively. The refined model was assessed using ProCheck [25] and MolProbity [26]. The average *B*-factors for all the atoms of the protein, Cu atoms and water molecules were 16.4, 13.6, and 30.4, respectively. The N- and C-terminal residues of the model had slightly elevated *B*-factors and somewhat diffuse electron density. In the final model, 10 residues (MENKNGTAAT) at the N-terminus and 11 residues (GEDDGSETSGH) at the C-terminus remained undefined because of the disorder. The refinement statistics are summarized in Table 1.

The crystals of the Δ1-68 mutant were obtained by using the hanging-drop vapor-diffusion technique. Droplets containing 10 mg/mL protein in 0.05 M Hepes-NaOH (pH 7.5) and 1.0 M ammonium formate were equilibrated over wells containing a reservoir solution [0.1 M Hepes-NaOH (pH 7.5) and 2.0 M ammonium formate]. The sample dishes were stored for crystallization in an incubator from 1 week to 1 month at 16.0 °C. The crystals were rinsed in a cryoprotectant solution (the reservoir solution supplemented with 30.0% v/v glycerol) before flash-freezing in liquid nitrogen. The diffraction data were collected at the Osaka University beamline BL44XU at SPring-8 (Hyogo, Japan) equipped with an MX225-HE detector (Rayonix). The image data were processed and scaled using the HKL package [27]. The crystals of the Δ1-68 mutant belong to the space group $P2_1$ with the following cell parameters: $a = 89.3$ Å, $b = 165.0$ Å, $c = 126.6$ Å, and $\beta = 102.3°$. The data set was 98.6% complete overall to a resolution of 1.77 Å with an R_{merge} of 8.0%. The data processing statistics are summarized in Table 1. The structure was determined through molecular replacement using the wt GkNiR structure as a search model after omitting the N-terminal region. Molrep [28] gave a unique solution, which was rigid-

Table 1
Crystallographic data and refinement statistics.

Data set	wt GkNiR	Δ1-68
Crystallographic statistics		
Wavelength, Å	1.0	0.9
Resolution, Å (outer shell)	18.9–1.30 (1.37–1.30)	42.7–1.77 (1.80–1.77)
Unique reflections	101,119	341,555
Completeness, % (outer shell)	95.2 (90.8)	98.6 (98.4)
R_{merge} (outer shell)	0.08 (0.36)	0.08 (0.56)
Data redundancy (outer shell)	3.5 (2.4)	3.3 (2.9)
Average I/σ (outer shell)	14.9 (2.4)	25.4 (2.1)
Refinement statistics		
Resolution range, Å	18.9–1.30	42.7–1.77
No. of reflections ($F > 0$)	96,275	323,635
Total no. of atoms (water)	2743 (334)	21279 (2029)
Completeness of data, %	95.1	98.4
R-factor[a](*R*-free)	0.182 (0.197)	0.172 (0.192)
RMS deviation[b]		
Bond, Å	0.009	0.013
Angle, °	1.3	1.4
Ramachandran plot		
Favored, %	97.7	98.6
Allowed, %	2.3	1.4

[a] *R*-factor = $\Sigma|F_{obs} - F_{calc}| / \Sigma F_{obs}$, and *R*-free was calculated on 5% of the reflections omitted at random.
[b] RMS deviations in bond lengths and angles are the deviations from ideal values.

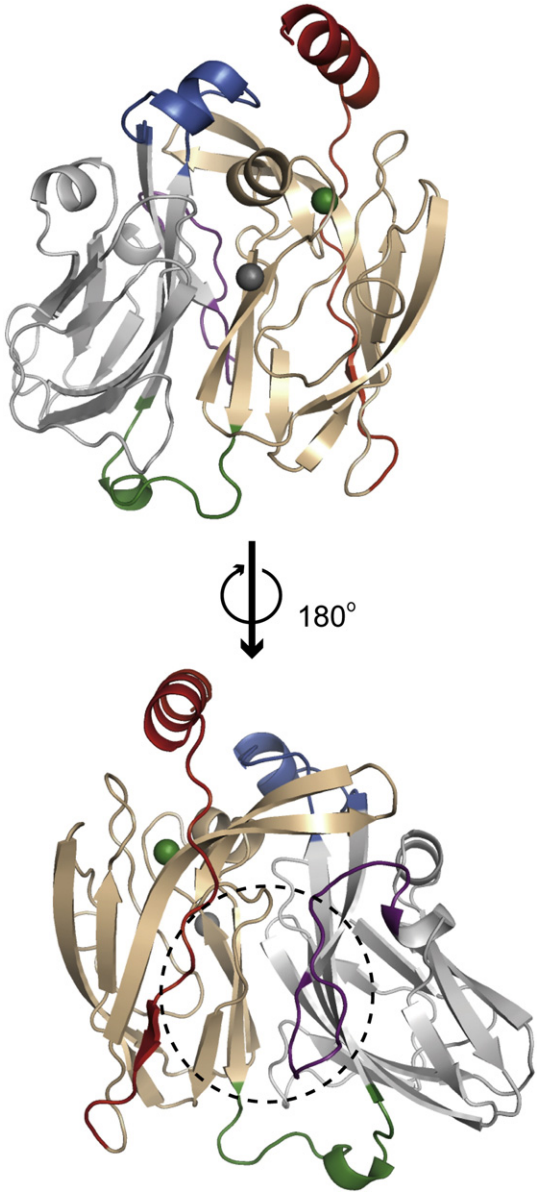

Fig. 1. Overall structure of the GkNiR monomeric subunit. Two cupredoxin domains are colored by light-gray and wheat. The "Linker", "Tower" and "Extra" loops are colored by green, blue, and purple, respectively. The unique N-terminal region is shown in red. Two Cu atoms (T1Cu and T2Cu) are represented as green and dark-gray balls. The *dashed-line* circle indicates the space occupied by the Extra loop in GkNiR, which is occupied by the N-terminal loop in the other CuNiRs (see Text and Fig. S1).

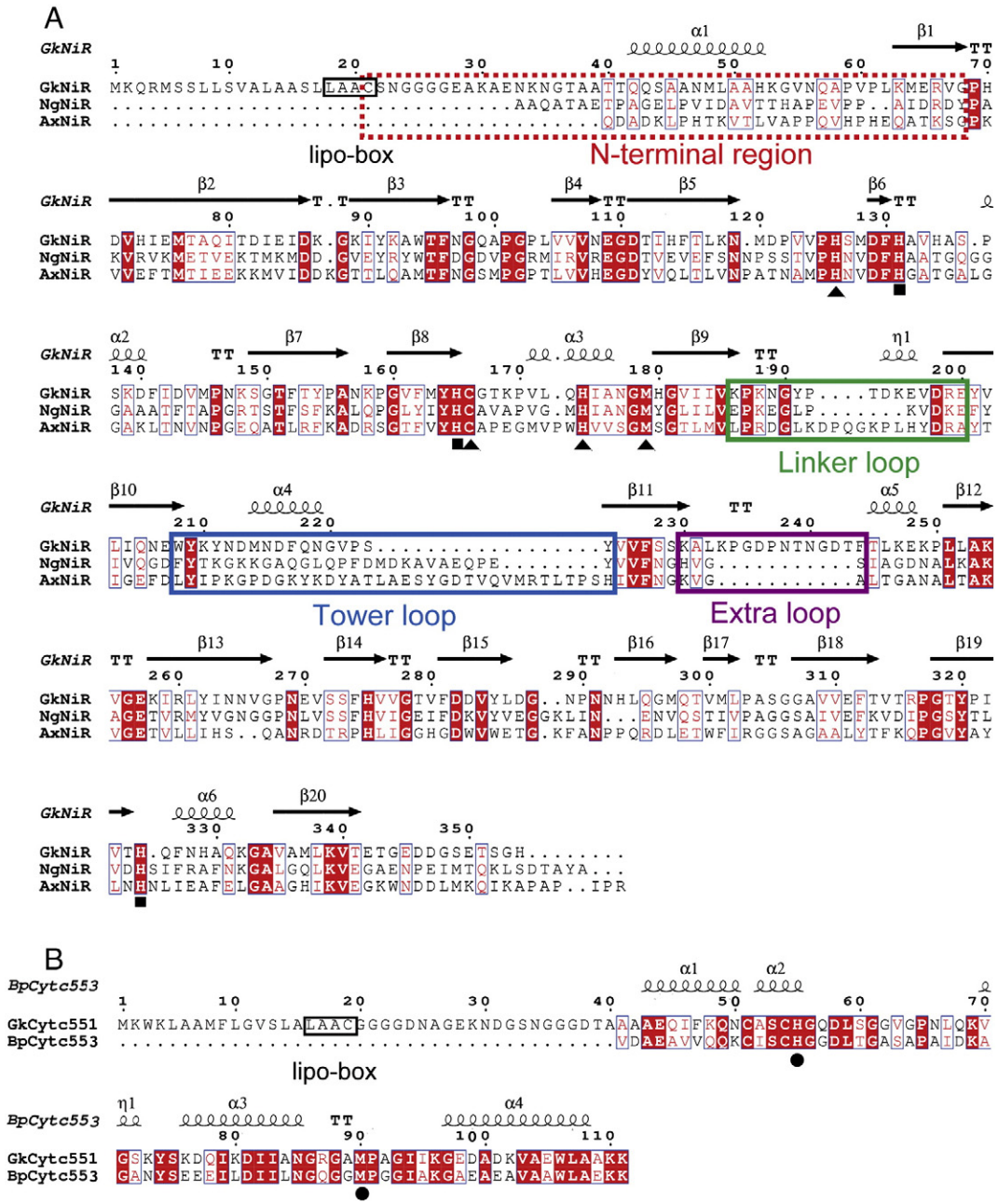

Fig. 2. Sequence comparisons of the proteins with homologues. (A) GkNiR and well-known CuNiRs. (B) GkCyt c_{551} and BpCyt c_{553}. Abbreviations and accession numbers are follows: GkNiR, CuNiR from *G. kaustophilus* HTA426 (UniProt code: Q5L1X8); NgNiR, CuNiR from *N. gonorrhoeae* (UniProt code: Q02219); AxNiR, CuNiR from *A. xylosoxidans* GIFU1051 (UniProt code: O68601); GkCyt c_{551}, Cyt c_{551} from *G. kaustophilus* HTA426 (UniProt code: Q5KV99); BpCyt c_{553}, Cyt c_{553} from *Bacillus pasteurii* (UniProt code: P82599). *ClustalW* was used to perform sequence alignment [40] and the figure was generated using the program ESPript [41]. Triangles, T1Cu ligands; squares, T2Cu ligands; circles, heme ligands. The characteristic N-terminal and loop regions are shown in colored boxes: dotted red, N-terminal region; green, Linker loop; blue, Tower loop; purple, Extra loop. The secondary structures for the present wt GkNiR model and BpCyt c_{553} (PDB code: 1c75) [42] are shown at the upper rows in (A) and (B), respectively. The sequence identity between GkCyt c_{551} and BpCyt c_{553} is 53%.

body refined using CNS [29]. Three trimer molecules (i.e., 9 monomeric subunits) were found in the asymmetric unit, and the resulting initial model gave an *R*-factor of 36% at a resolution of 2.5 Å after rigid-body refinement and minimization. Several stages of refinement were performed using Coot and Refmac5. The model was then thoroughly examined for possible errors using both maps at contour levels of 1.2σ ($2F_O-F_C$) and $\pm 3.5\sigma$ (F_O-F_C). The structure was refined to obtain *R*-factor and *R*-free values of 0.17 and 0.19, respectively; the root-mean-squared deviations (RMSDs) of the bond lengths and angles from the ideal values were 0.013 Å and 1.4°, respectively. The refined model was assessed using Procheck and Molprobity. The average *B*-factors for all the atoms of each monomer (chain A, B, C, D, E, F, G, H, and I) and water molecules were 24.4, 24.5, 23.8, 25.0, 24.0, 23.5, 24.7, 27.0, 25.1 and 37.5 $Å^2$, respectively. Some amino acid residues of the model showed slightly elevated *B*-factors and somewhat diffuse electron density. In the final model, two residues (MP) at the N-termini for chains A-H and three residues (MPH) at the N-terminus for chain I, and 12 residues (TGEDDGSETSGH) at the C-termini for all chains were undefined because of the disorder. The refinement statistics are summarized in Table 1.

2.5. Stopped-flow kinetics

Stopped-flow kinetics experiments of the ET reaction from the reduced Cyt c_{551} to CuNiR were performed in a 10 mM Tris–HCl buffer (pH 8.0) at 25 °C under anaerobic conditions. To maintain pseudo-first-order conditions, the concentration ratios of CuNiR to Cyt c_{551}

were always more than 10 times [CuNiR, 30 μM (as a monomer); Cyt c_{551}, 1.0 μM]. The pseudo-first-order rate constants (k_{obs}) were obtained by fitting the experimental data with a single exponential function. The kinetic traces were acquired with an RA-2000 stopped-flow spectrophotometer (Otsuka Electronics) using the single-wavelength mode at the wavelength 420 nm [10].

3. Results and discussion

3.1. Overall structure of GkNiR

In the previous preliminary X-ray crystallographic experiments [16], one monomeric subunit of wt GkNiR molecule has been found in the asymmetric unit of the rhombohedral *R*3 crystal, organized into a physiologically relevant homo-trimeric structure related to a crystallographic three-fold axis. The structure was refined to give an *R*-factor of 18.2% (*R*-free = 19.7%) at a 1.3-Å resolution. The final model consists of 303 connected amino acid residues (from Thr41 to Thr343), two Cu^{2+} atoms, three Zn^{2+}, two Na^{+}, one SO_4^{-}, and 334 water molecules. All the extra ions, Zn^{2+}, Na^{+}, and SO_4^{-} were localized at the molecular surface of GkNiR, probably due to the crystallization conditions. Several statistical indicators confirm to the quality of the structure. For example, 97.7% of the residues occupy the favored region of the Ramachandran plot and there are no residues in the disallowed regions. The RMS deviations of the bond lengths and angle degrees from the ideal values are 0.009 Å and 1.3°, respectively (Table 1).

The overall structure for GkNiR can be roughly divided with the N- and C-terminal domains, each of which folds into a Greek key β-barrel domain (Fig. 1). A sequence alignment for the GkNiR model with Class-I and II CuNiRs is shown in Fig. 2A. As would be predicted by comparing the sequences [16], the Linker and Tower loops of GkNiR are shorter than those found in Class-I CuNiRs. Interestingly, they also clearly differ from those of NgNiR, a typical Class-II CuNiR. For example, the Linker loop of GkNiR is longer than that of NgNiR by three residues, and a one-turned 3_{10} helix structure which is not seen in the Linker loop of NgNiR is observed in the GkNiR structure (Figs. 1, 2A and Fig. S1). Generally, the Tower loop of Class-I CuNiR adopts a random-coiled structure leading to a four-turned α-helix, which extended toward the T1Cu. Moreover, the eight-residues deletion in the corresponding Tower loop in the Class-II CuNiR results in a shortened α-helix with one and a half turns [8]. The 18-residues deletion in the Tower loop region of GkNiR results in a shorter structure. In particular, the random-coiled region of the Tower loop of GkNiR is shorter than those of all the other CuNiRs. Moreover, the unique Extra loop structure suggested by a previous sequence alignment analysis [16], composed of 11 residues of the downstream of the Tower loop, was also confirmed in the GkNiR model (Figs. 1 and 2A). Here, the Extra loop is more than 20 Å apart from both T1Cu and T2Cu and, that it is positioned in the space occupied by the N-terminal polypeptides of all CuNiRs. As mentioned below, the position and the structure of the N-terminus of GkNiR is distinct from other CuNiRs and it does not occupy the same space (Fig. 1 and Fig. S1). Besides the existence of the extra 11 residues in the downstream region of the deleted Tower loop, the overall β-barrel structure of GkNiR well-overlaps with the tertiary structures of other CuNiRs, including Class-I CuNiRs.

The most unique feature of the structure of GkNiR is its novel N-terminal arm structure composed of 28 residues (from Thr41 to Gly68). While both the N- and C-termini of the typical trimeric CuNiRs are directed towards the southern side of the molecule (Fig. S1), the N-terminus of GkNiR extends in the direction of the northern side of the surface of T1Cu and forms a α-helix structure (Fig. 3A). The place where this α-helix is positioned in CuNiRs corresponds to the interaction surface with the physiological redox-partner proteins [9,10] and the superposition of GkNiR on the well-known complex structure of AxNiR with its partner AxCyt c_{551} indicates that the N-terminal α-helix of GkNiR partially overlaps with AxCyt c_{551} (Fig. 3B). Similarly, overlapping of the helix region to the fused domains corresponding to the partner protein is also observed in the superposition on the natural fusion-types CuNiR structures [11–13] (Fig. S2). Furthermore, to evaluate how this unique structure affects the overall structure of GkNiR, the crystal structure of the N-terminal 68-residues deletion mutant (Δ1-68) was determined at 1.8-Å resolution (Table 1 and Fig. S3). The refined model of the mutant shows a very good consistency with the wt GkNiR model, clearly indicating that the folding of the core region of GkNiR is independent on the unique N-terminal region.

3.2. The Cu-binding sites

The T1Cu is positioned approximately 6-Å below the molecular surface of the GkNiR molecule. Two His nitrogen atoms (His126 Nδ[1] and His174 Nδ[1]), and two sulfur atoms, one from Cys166 (Sγ) and the other from Met179 (Sδ), coordinate the Cu atom (Fig. 4). Their His and

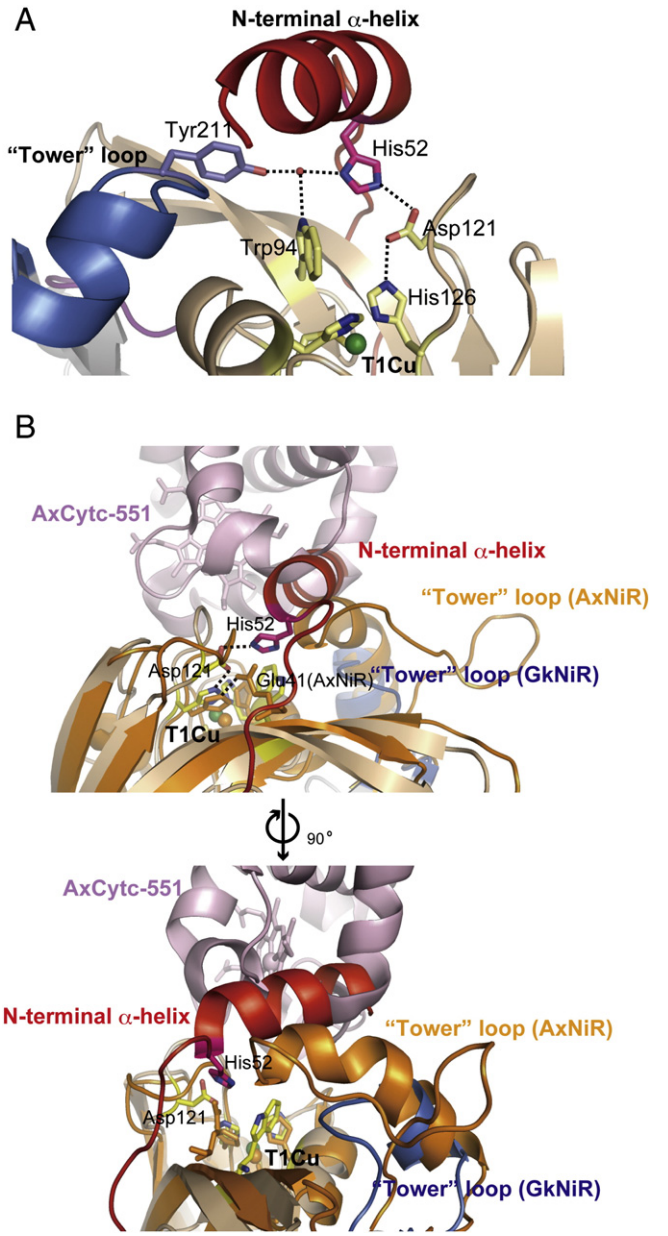

Fig. 3. The unique α-helix structure in the N-terminal region. (A) Zoom-up view of the unique α-helix location. The *dotted-lines* mean the hydrogen bonds network. (B) Superposition of the GkNiR model on the complex structure of AxNiR with AxCyt c_{551}. AxNiR and AxCyt c_{551} are shown as orange and light pink colored, respectively. The color scheme for GkNiR is same to the pattern used in Fig. 1.

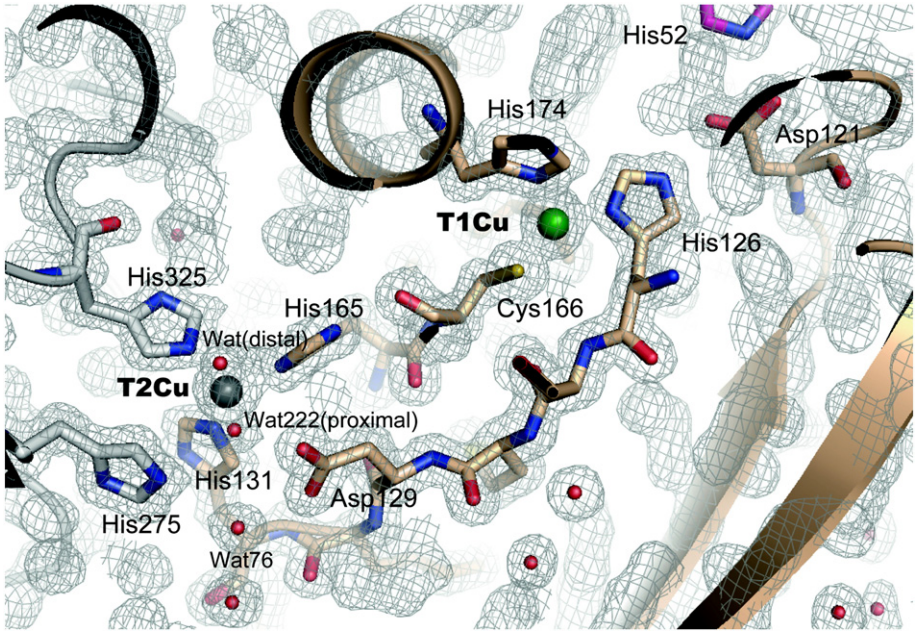

Fig. 4. The Cu-binding sites. T1Cu, T2Cu, and their ligand residues are shown as a *ball-and-stick* representation. The $2F_O–F_C$ difference Fourier electron density map was overlayed on the structure as a contour level 1σ.

Cys residues are positioned approximately in plane with the Cu atom adopting near trigonal geometry, while the weaker Met adopts an axial coordination. Ligand distances and bond geometries are presented in Table 2. The two His of four ligands are the nearest the molecular surface; the Nε^2 atom of His174 is exposed to the solvent and forms a hydrogen bond (2.77 Å) with a water molecule (Wa28), the Nε^2 atom of His126 forms a hydrogen bond (2.73 Å) with the Oδ^2 atom of an aspartate (Asp121), while the corresponding latter His forms a hydrogen bond with the Glu Oε^1 atom in the reported all CuNIRs. Interestingly, the Oδ^1 atom of Asp121 also forms a hydrogen bond with His52 in the unique N-terminal α-helix (Fig. 3A). Of the three planes in the imidazole ring of His126, the plane occupied by the Oδ^1, Oδ^2 and Cγ atoms of Asp121, and the imidazole ring of His52 are approximately co-planar. It is clearly different from the structure of the other CuNiRs in that the imidazole ring of the His corresponding to His126 in GkNiR and the plane occupied by Oε^1, Oε^2, and Cδ of the Glu forming the hydrogen bond with the His are nearly orthogonal (Fig. 3B). Moreover, His52 can interact with Tyr211 in the Tower loop and to Trp94 above the T1Cu site through the hydrogen bond network (Fig. 3A). The main chain for His126 also forms hydrogen bonds with the amide N (2.71 Å) and carbonyl O (3.11 Å) of the nearby Val144. These hydrogen bond networks are unique to GkNiR and may contribute to the reactivity of GkNiR. Furthermore, the Sγ atom of Cys166 forms hydrogen bonds with the amide N (3.50 Å) of Ser127, and the amide N of Gly167 (3.39 Å). These distances are slightly longer than those of the corresponding hydrogen bonds in AxNiR, in which the ligand Cys130 forms hydrogen bonds with the amide N (3.34 Å) of Asn90 and the amide N of Ala131 (3.33 Å). Moreover, the Sγ atom of Cys166 in GkNiR can also interact with the amide N and Oγ of Thr168 (3.57 Å and 3.48 Å respectively). These interactions are not found in the Class-I CuNiRs.

The catalytic T2Cu site is located in the inter-subunit cleft at about 12 Å from the molecular surface and is ligated with the Nε^2 atoms of three His residues, two provided by the N-terminal domain of one monomeric subunit (His131 and His165), and the third provided by the C-terminal domain of the adjacent monomer (His325), forming a distorted tetrahedral-like geometry. Ligand distances and bond geometries are presented in Table 2. T2Cu is approximately 12.5 Å apart from T1Cu, and the two copper sites are connected through a peptide chain incorporating the residues His165, a T2Cu ligand, and Cys166, a T1Cu ligand. The key residues involved in the catalytic function (Asp129 and

Table 2
Bond lengths and angles for Cu-binding sites.

Parameter	wt GkNiR
T1Cu ligand distances (Å)	
Cu–His-126 Nδ^1	2.07
Cu–Cys-166 Sγ	2.13
Cu–His-174 Nδ^1	2.03
Cu–Met-179 Sδ	2.61
T1Cu ligand angles (°)	
His-174 Nδ^1–Cu–Met-179 Sδ	117
Cys-166 Sγ–Cu–His-126 Nδ^1	139
His-126 Nδ^1–Cu–Met-179 Sδ	82
Cys-166 Sγ–Cu–Met-179 Sδ	113
Cys-166 Sγ–Cu–His-174 Nδ^1	103
His-174 Nδ^1–Cu–His-126 Nδ^1	99
T2Cu ligand distances (Å)	
Cu–His-131 Nε^2	1.95
Cu–His-165 Nε^2	2.08
Cu–His-325 Nε^2	2.04
Cu–water $O_{(proximal)}/O_{(distal)}$	1.92/2.53
T2Cu ligand angles (°)	
His-131 Nε^2–Cu–His-165 Nε^2	112
His-131 Nε^2–Cu–His-325 Nε^2	98
His-165 Nε^2–Cu–His-325 Nε^2	103
His-131 Nε^2–Cu–water $O_{proximal}$	97
His-165 Nε^2–Cu–water $O_{proximal}$	104
His-325 Nε^2–Cu–water $O_{proximal}$	139
His-131 Nε^2–Cu–water O_{distal}	154
His-165 Nε^2–Cu–water O_{distal}	92
His-325 Nε^2–Cu–water O_{distal}	86

Table 3
Steady-state kinetics parameters for nitrite reductase activity.

	k_{cat} (s^{-1})	K_m (μM)	k_{cat}/K_m (s^{-1} μM^{-1})
GkNiR	$(7.96 \pm 0.49) \times 10^2$	79 ± 20	10.1
AxNiR	$(1.51 \pm 0.06) \times 10^3$	42 ± 6	36.0

His275) are conserved in GkNiR, but the highly-conserved Ile residue in the active site, which controls the mode of nitrite binding in CuNiRs [30,31], is substituted by a Val277 in GkNiR. In an earlier study, Murphy et al. demonstrated that Ile could be replaced with Val [31]. A water molecule and/or a hydroxyl ion are bound to the T2Cu at the two coordination sites; one is hydrogen-bonded to Asp129 and the other is not (Fig. 4). The side-chain $O\delta^1$ atom of Asp129 forms a hydrogen bond (2.42 Å) with Wat222, the water ligand of T2Cu, and $O\delta^2$ with Wat76 (2.83 Å), the water forming a hydrogen bond network leading to the water ligand bound to T2Cu. A similar hydrogen bonds environment around T2Cu is also conserved in the Δ1-68 mutant structure, although some water molecules are replaced with two formate molecules originating during the crystallization condition. Curiously, a half-occupancy formate anion directly bound to T2Cu at the distal coordination site detached from Asp129 in the mutant structure (Fig. S4). Since formic acid and Asp129 should be mostly deprotonated at pH 7.5 under the present crystallization condition, it is likely that they become separated due to the considerable electrostatic or lone pair repulsion. Moreover, the imidazole rings of His131 and His275 are close and approximately parallel. The distance between $N\varepsilon^2$ of His275 and $N\varepsilon^2$ of His131, and $C\varepsilon^1$ of His275 and $N\delta^1$ of His131 are especially close (3.24 Å and 3.51 Å, respectively), suggesting the existence of a π-π interaction between both residues.

Additionally, the T1Cu and T2Cu geometric parameters for Δ1-68 mutant are mostly within errors to those of the wt GkNiR model (Table S1), indicating that the loss of the unique N-terminal region does not affect their Cu-coordinated structures.

3.3. Functional characterization of GkNiR

The nitrite-reducing activity of GkNiR was estimated by a standard assay for CuNiR using methyl viologen as the artificial electron donor [18]. The resultant k_{cat} was 796 ± 49 s^{-1} at pH 6.5 at 25.0 °C, corresponding to about half of that for AxNiR under the same condition (Table 3). The redox potential (E_m) value of GkNiR was evaluated by spectrochemical titration using Fe(II)/(III)-EDTA (E_m = +120 mV vs. normal hydrogen electrode, NHE) as a redox buffer [32–35]. The oxidation state of the GkNiR was monitored by the absorption of the peak centered at 600 nm (Fig. 5A). The analysis of the data using a Nernst Equation (Fig. 5B) yield an E_m value of +194 ± 1 mV and a value of n = 1.5 ± 0.1 for the number of electrons transferred during the redox reaction. On the other hand, in the case of AxNiR, it expectedly yield a value of n = 1.9 ± 0.1 and an E_m value of +214 ± 1 mV (Fig. 5B). The n (>1) value means that electron flow exists between T1Cu and T2Cu, and that their redox potentials are close. The difference on the redox behaviors between AxNiR and GkNiR maybe due to the different hydrogen bonds network around the Cu sites as seen in the present crystal structure, because the hydrogen bonds around the metal site greatly affects the redox potentials [36]. Moreover, by comparing the n values, it is suggested that the balance of redox potential between T1Cu and T2Cu in GkNiR differs from those in AxNiR, otherwise GkNiR might be in several state, one of which operates through a gated mechanism on the intramolecular ET between T1Cu and T2Cu, triggering nitrite binding and/or protonation [37]. It is a next subject to identify the detailed mechanism.

Furthermore, to elucidate the function of the N-terminal α-helix upon the interprotein ET reaction, the kinetic analysis of ET between CuNIRs and its physiological electron donors was carried out by stopped-flow techniques at 25 °C. Not only AxNiR, AxCyt c_{551} and wt GkNiR but also Δ1-51, a N-terminal α-helix deletion mutant of GkNiR, and GkCyt c_{551}, were used and experiments on all six combinations of CuNIRs and cytochromes were performed. The results of the six combinations are shown in Fig. 6 and Table 4. The pseudo first-order ET rate constant (k_{obs}) of AxCyt c_{551}-GkNiR is about three orders of magnitude lower than that of AxCyt c_{551}-AxNiR, while k_{obs} of AxCyt c_{551}-Δ1-51 is about an order of magnitude larger than that of AxCyt c_{551}-GkNiR. On the other hand, the comparison of k_{obs} of GkCyt c_{551}-GkNiR with that of GkCyt c_{551}-Δ1-51 revealed a 2.8-fold faster ET. These kinetics results clearly indicate that the Δ1-51 mutant loosely recognizes the partner. Because it is assumed that the rate-determining step is the protein–protein association process, the observed differences between the k_{obs} measured in the present experiment reflect the differences of the association processes in which the electron-transfer complexes are formed transiently. The classical Marcus theory describes the rate of the ET accompanying the increase of the distance between two redox centers as an exponential decay [38]. In other words, the dramatic decrease in the rate of the ET implies a slight increase of the distance between the two proteins. Accordingly, it seems that the N-terminal α-helix of GkNiR prevents AxCyt c_{551} from approaching the neighborhood of the GkNiR T1Cu to form the electron-transfer complex, as predicted by structural analysis. On the other hand, the

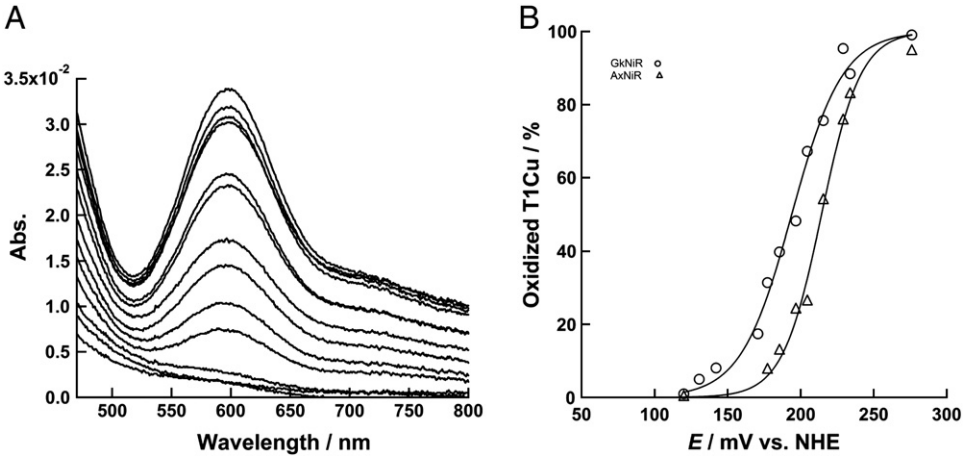

Fig. 5. Redox titration of GkNiR. (A) Absorption changes during the titration. The reaction mixture contained 20 μM GkNiR and 2 mM Fe(II)/(III)-EDTA (E_m = +120 mV vs. NHE) in 10 mM sodium phosphate buffer (adjusted to the 20 mM of ionic strength with NaCl), pH 7.0, at 25 °C. The Fe(II)/(III)-EDTA was prepared by mixing EDTA solution with $FeCl_2$ or $FeCl_3$ in which EDTA was maintained in at least 20% excess over iron. The oxidized CuNiRs were anaerobically added to the various ratios of Fe(II)/(III)-EDTA mixture solutions in a glove box. (B) Analysis of data by an Equation, $E = E_m + (RT/nF) \times \ln([GkNiR_{oxidized}] / [GkNiR_{reduced}])$. The plots of titration of AxNiR (triangle) are also shown to compare with those of GkNiR (square).

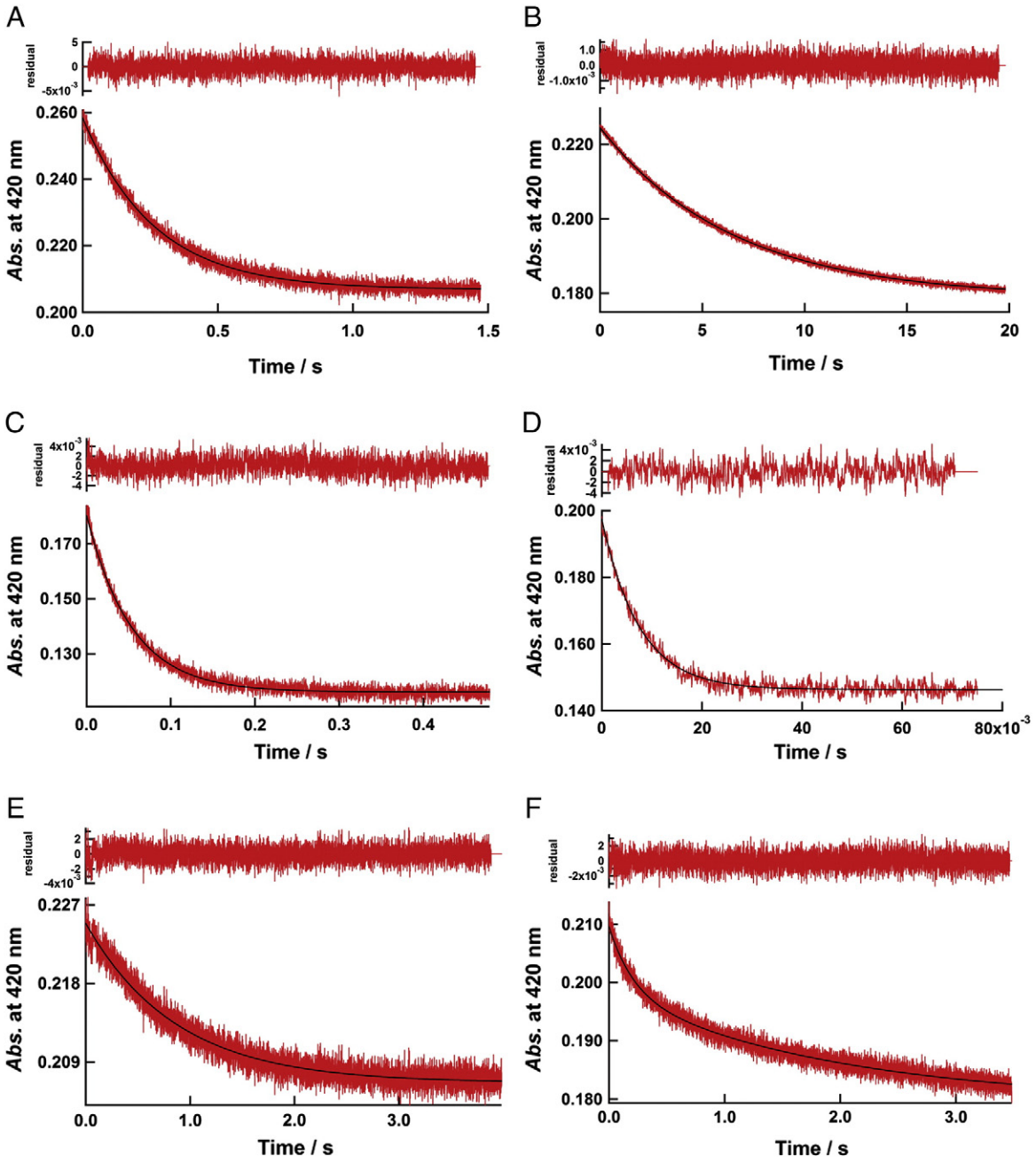

Fig. 6. Stopped-flow kinetics between CuNiRs and Cyts c_{551}. (A) GkNiR vs. GkCyt c_{551}. (B) GkNiR vs. AxCyt c_{551}. (C) AxNiR vs. GkCyt c_{551}. (D) AxNiR vs. AxCyt c_{551}. (E) Δ1-51 mutant vs. GkCyt c_{551}. (F) Δ1-51 mutant vs. AxCyt c_{551}.

comparison of the k_{obs} of GkCyt c_{551}-GkNiR with that of GkCyt c_{551}-Δ1-51 shows that the former combination achieved 2.8-fold faster ET, meaning that the intermolecular electron transfer between the native proteins pair is faster than that between GkCyt c_{551} and Δ1-51 mutant. This suggests not only that the N-terminal α-helix structure does not prevent the protein–protein interaction between GkCyt c_{551} and GkNiR but also that it is necessary to achieve an effective electron transfer in physiological redox-partners pairs.

Furthermore, both proteins, GkNiR and GkCyt c_{551}, are likely to express as membrane-anchored protein in the living *G. kaustophilus* cell, because they have a lipo-box motif [20] in the sequences (Fig. 2). The present structure and kinetics data clearly indicate that they can form transiently an ET complex using the similar interaction sites to the already-known CuNiR:Cyt c_{551} complex structure. Considering that both proteins are anchored to the membrane, the complex model has been constructed based on the already-known complex structure of AxNiR with AxCyt c_{551} (Fig. S5). In this hypothetical model, the Cyt c_{551}-binding site on the GkNiR molecular surface is accessible for GkCyt c_{551} to follow the efficient ET at the interspace between the GkNiR molecule and lipid bilayer, even if they are anchored to the membrane. NgNiR is also known as a membrane-anchored protein similar to GkNiR [39]. The N-terminus of NgNiR is interestingly located at southern side opposite to GkNiR as shown in Fig. S1, which may reflect the difference of the orientation to the membrane and recognition mechanism with redox-partner proteins on the outer membrane. Further structure analysis of the transient GkNiR:Cyt c_{551} complex would be necessary to identify the detailed structural basis for *Geobacillus* CuNiR–Cyt c_{551} system.

Table 4
Parameters for interprotein ET kinetics.

	GkCyt c_{551}	AxCyt c_{551}
GkNiR	3.68 ± 0.39	$(1.70 \pm 0.19) \times 10^{-1}$
AxNiR	$(2.01 \pm 0.14) \times 10$	$(1.09 \pm 0.17) \times 10^{2}$
Δ1-51	1.29 ± 0.17	[a]5.99 ± 0.46 (41%), 0.52 ± 0.08 (59%)

Pseudo-first-order ET rate constants (s^{-1}) between CuNiRs and the redox partners measured using stopped-flow spectrophotometer (see Materials and methods).
[a] The values were obtained by fitting the decay curve with a double exponential function. Relative amplitude is given in parenthesis.

4. Conclusion

In the present study, we performed X-ray crystallographic analysis of CuNiR from a thermophilic Gram-positive bacterium *Geobacillus kaustophilus* and determined its tertiary structure at 1.3-Å resolution. The structural result revealed novel structures including the shortened Tower loop, an Extra loop, an N-terminal α-helix and hydrogen bond networks around the T1Cu site. The nitrite reductase activity, stopped-flow kinetics, and redox titration analyses provided evidence of a structure-function relationship in the present GkNiR model. In particular, the N-terminal α-helix unique to GkNiR contributes to the specific partner recognition to yield an effective interprotein electron transfer. The present knowledge obtained through the GkNiR structure solved at 1.3-Å resolution and functional analysis might shed light on the previously unknown structural, functional and evolutionary diversities of CuNiRs. Additionally, recent genomics studies have shown that there are other unknown CuNiRs that are expected to have novel structures on the basis of their amino acid sequences. Thus, if these structures will be elucidated in the future, we could understand the functional variety of CuNiRs and their evolutionary history at a deeper level. We believe that the present study provides important clue to this understanding as well.

Acknowledgements

We thank Prof. A. Nakagawa, Drs. M. Suzuki, and E. Yamashita (BL44XU at SPring-8) for their kind support in the collection of X-ray data (proposal Nos. 2011B6634 and 2012A6736 to M.N.). The MX225-HE detector used in this study is financially supported by the Academia Sinica and National Synchrotron Radiation Research Center (Taiwan, ROC). This study was supported in part by Grant-in-Aids for Encouragement of Young Scientists 20750137 and 23750190 (to M.N.) from the Ministry of Education, Culture, Sports, Science and Technology of Japan. The plasmid pEC86 was a generous gift from Dr. Julie M. Stevens (University of Oxford, UK). We also thank an emeritus Prof. S. Suzuki for discussion.

Appendix A. Supplementary data

Supplementary data to this article can be found online at http://dx.doi.org/10.1016/j.bbabio.2014.01.004.

References

[1] D.E. Canfield, A.N. Glazer, P.G. Falkowski, The evolution and future of earth's nitrogen cycle, Science 330 (2010) 192–196.
[2] S. Demanéche, L. Philippot, M.M. David, E. Navarro, T.M. Vogel, P. Simonet, Characterization of denitrification gene clusters of soil bacteria via a metagenomic approach, Appl. Environ. Microbiol. 75 (2009) 534–537.
[3] E. Piña-Ochoa, S. Hogslung, E. Geslin, T. Cedhagen, N.P. Revsbech, L.P. Nielsen, M. Schweizer, F. Jorissen, S. Rysgaard, N. Risgaard-Petersen, Widespread occurrence of nitrate storage and denitrification among Foraminifera and Gromiida, Proc. Natl. Acad. Sci. U. S. A. 107 (2010) 1148–1153.
[4] W.G. Zumft, Cell biology and molecular basis of denitrification, Microbiol. Mol. Biol. Rev. 61 (1997) 533–616.
[5] A.E. Santoro, A.B. Boehm, C.A. Francis, Denitrifier community composition along a nitrate and salinity gradient in a coastal aquifer, Appl. Environ. Microbiol. 72 (2006) 2102–2109.
[6] J.W. Godden, S. Turley, D.C. Teller, E.T. Adman, M.Y. Liu, W.J. Payne, J. LeGall, The 2.3 Å X-ray structure of nitrite reductase from *Achromobacter cycloclastes*, Science 253 (1991) 438–442.
[7] E.I. Solomon, Spectroscopic methods in bioinorganic chemistry: blue to green to red copper sites, Inorg. Chem. 45 (2006) 8012–8025.
[8] M.J. Boulanger, M.E. Murphy, Crystal structure of the soluble domain of the major anaerobically induced outer membrane protein (AniA) from pathogenic Neisseria: a new class of copper-containing nitrite reductase, J. Mol. Biol. 315 (2002) 1111–1127.
[9] M.D. Vlasie, R. Fernández-Busnadiego, M. Prudêncio, M. Ubbink, Conformation of pseudoazurin in the 152 kDa electron transfer complex with nitrite reductase determined by paramagnetic NMR, J. Mol. Biol. 375 (2008) 1405–1415.
[10] M. Nojiri, H. Koteishi, T. Nakagami, K. Kobayashi, T. Inoue, K. Yamaguchi, S. Suzuki, Structural basis of inter-protein electron transfer for nitrite reduction in denitrification, Nature 462 (2009) 117–120.
[11] M. Nojiri, Y. Xie, T. Inoue, T. Yamamoto, H. Matsumura, K. Kataoka, Deligeer, K. Yamaguchi, Y. Kai, S. Suzuki, Structure and function of a hexameric copper-containing nitrite reductase, Proc. Natl. Acad. Sci. U. S. A. 104 (2007) 4315–4320.
[12] A. Tsuda, R. Ishikawa, H. Koteishi, K. Tange, Y. Fukuda, K. Kobayashi, T. Inoue, M. Nojiri, Structural and mechanistic insights into the electron flow through protein for cytochrome *c*-tethering copper nitrite reductase, J. Biochem. 154 (2013) 51–60.
[13] S.V. Antonyuk, C. Han, R.R. Eady, S.S. Hasnain, Structures of protein-protein complexes involved in electron transfer, Nature 496 (2013) 123–126.
[14] L. Feng, W. Wang, J. Cheng, Y. Ren, G. Zhao, C. Gao, Y. Tang, X. Liu, W. Han, X. Peng, R. Liu, L. Wang, Genome and proteome of long-chain alkane degrading *Geobacillus thermodenitrificans* NG80-2 isolated from a deep-subsurface oil reservoir, Proc. Natl. Acad. Sci. U. S. A. 104 (2007) 5602–5607.
[15] I. Verbaendert, N. Boon, P. De Vos, K. Heylen, Denitrification is a common feature among members of the genus *Bacillus*, Syst. Appl. Microbiol. 34 (2011) 385–391.
[16] Y. Fukuda, T. Tamada, H. Takami, S. Suzuki, T. Inoue, M. Nojiri, Cloning, expression, purification, crystallization and preliminary X-ray crystallographic study of GK0767, the copper-containing nitrite reductase from *Geobacillus kaustophilus*, Acta Crystallogr. F67 (2011) 692–695.
[17] E. Arslan, H. Schulz, R. Zufferey, P. Kunzler, L. Thöny-Meyer, Overproduction of the *Bradyrhizobium japonicum c*-type cytochrome subunits of the *cbb*3 oxidase in *Escherichia coli*, Biochem. Biophys. Res. Commun. 251 (1998) 744–747.
[18] K. Kataoka, H. Furusawa, K. Takagi, K. Yamaguchi, S. Suzuki, Functional analysis of conserved aspartate and histidine residues located around the type 2 copper site of copper-containing nitrite reductase, J. Biochem. 127 (2000) 345–350.
[19] O. Emanuelsson, S. Brunak, G. von Heijne, H. Nielsen, Locating proteins in the cell using TargetP, SignalP and related tools, Nat. Protoc. 2 (2007) 953–971.
[20] M.M. Babu, M.L. Priya, A.T. Selvan, M. Madera, J. Gough, L. Aravind, K. Sankaran, A database of bacterial lipoproteins (DOLOP) with functional assignments to predicted lipoproteins, J. Bacteriol. 188 (2006) 2761–2773.
[21] S.P. Lei, H.C. Lin, S.S. Wang, J. Callaway, G. Wilcox, Characterization of the *Erwinia carotovora* pelB gene and its product pectate lyase, J. Bacteriol. 169 (1987) 4379–4383.
[22] Deligeer, K. Kataoka, K. Yamaguchi, S. Suzuki, Spectroscopic and electrochemical properties of cytochrome c_{551} from *Alcaligenes xylosoxidans* GIFU1051, Bull. Chem. Soc. Jpn. 73 (2000) 1839–1840.
[23] P. Emsley, B. Lohkamp, W.G. Schott, K. Cowtan, Features and development of Coot, Acta Crystallogr. D66 (2010) 486–501.
[24] G.N. Murshudov, A.A. Vagin, E.J. Dodson, Refinement of macromolecular structures by the maximum-likelihood method, Acta Crystallogr. D53 (1997) 240–255.
[25] R.A. Laskowski, M.W. MacArthur, D.S. Moss, J.M. Thornton, *PROCHECK*: a program to check the stereochemical quality of protein structures, J. Appl. Crystallogr. 26 (1993) 283–291.
[26] S.C. Lovell, I.W. Davis, W.B. Arendall III, P.I.W. de Bakker, J.M. Word, M.G. Prisant, J.S. Richardson, D.C. Richardson, Structure validation by Cα Geometry: ϕ, ψ and Cβ deviation, Proteins 50 (2003) 437–450.
[27] Z. Otwinowski, W. Minor, Processing of X-ray diffraction data collected in oscillation mode, Methods Enzymol. 276 (1997) 307–326.
[28] A. Vagin, A. Teplyakov, *MOLREP*: an automated program for molecular replacement, J. Appl. Crystallogr. 30 (1997) 1022–1025.
[29] A.T. Brünger, P.D. Adams, G.M. Clore, W.L. DeLano, P. Gros, R.W. Grosse-Kunstieve, J.S. Jiang, J. Kuszewski, M. Nilges, N.S. Pannu, R.J. Read, L.M. Rice, T. Simonson, G.L. Warren, Crystallography & NMR system: a new software suite for macromolecular structure determination, Acta Crystallogr. D54 (1998) 905–921.
[30] A.C. Merkle, N. Lehnert, The side-on copper(I) nitrosyl geometry in copper nitrite reductase is due to steric interactions with isoleucine-257, Inorg. Chem. 48 (2009) 11504–11506.
[31] M.J. Boulanger, M.E.P. Murphy, Directing the mode of nitrite binding to a copper-containing nitrite reductase from *Alcaligenes faecalis* S-6: characterization of an active site isoleucine, Protein Sci. 12 (2003) 248–256.
[32] R. Belcher, D. Gibbons, T.S. West, The effect of ethylenediaminetetraacetic acid on the ferrous/ferric and cuprous/cupric redox systems, Anal. Chim. Acta. 12 (1955) 107–114.
[33] H.J. Wijma, I. MacPherson, O. Farver, E.I. Tocheva, I. Pecht, M. Verbeet, M.E.P. Murphy, G.W. Canters, Effect of the methionine ligand on the reorganization energy of the type-1 copper site of nitrite reductase, J. Am. Chem. Soc. 129 (2007) 519–525.

[34] P.L. Dutton, Redox potentiometry: Determination of midpoint potentials of oxidation-reduction components of biological electron-trabsfer systems, Methods Enzymol. 54 (1978) 411–435.
[35] C.L. Coyle, H.B. Gray, Kinetic studies of the reduction of *Pseudomonas aeruginosa* ferricytochrome c_{551} by $Fe(EDTA)^{2-}$, Biochem. Biophys. Res. Commun. 73 (1976) 1122–1127.
[36] N.M. Marshall, D.K. Garner, T.D. Wilson, Y.G. Gao, H. Robinson, M.J. Nilges, Y. Lu, Rationally tuning the reduction potential of a single cupredoxin beyond the natural range, Nature 462 (2009) 113–116.
[37] N.G. Leferink, C.R. Pudney, S. Brenner, D.J. Heyes, R.R. Eady, S.S. Hasnain, S. Hay, S.E. Rigby, N.S. Scrutton, Gating mechanisms for biological electron transfer: integrating structure with biophysics reveals the nature of redox control in cytochrome P450 reductase and copper-dependent nitrite reductase, FEBS Lett. 586 (2012) 578–584.
[38] R.A. Marcus, N. Sutin, Electron transfers in chemistry and biology, Biochim. Biophys. Acta 811 (1985) 265–322.
[39] G.T. Hoehn, V.L. Clark, The major anaerobically induced outer membrane protein of *Neisseria gonorrhoeae*, Pan 1, is a lipoprotein, Infect. Immun. 60 (1992) 4704–4708.
[40] J.D. Thompson, D.G. Higgins, T.J. Gibson, CLUSTAL W: improving the sensitivity of progressive multiple sequence alignment through sequence weighting, position-specific gap penalties and weight matrix choice, Nucleic Acids Res. 22 (1994) 4673–4680.
[41] P. Gouet, E. Courcelle, D.I. Stuart, F. Métoz, ESPript: analysis of multiple sequence alignments in PostScript, Bioinformatics 15 (1999) 305–308.
[42] S. Benini, A. González, W.R. Rypniewski, K.S. Wilson, J.J. Van Beeumen, S. Ciurli, Crystal structure of oxidized *Bacillus pasteurii* cytochrome c_{553} at 0.97-Å resolution, Biochemistry 39 (2000) 13115–13126.